submitted to The Astrophysical Journal Letters



# EVIDENCE FOR AN EARLY HIGH-ENERGY AFTERGLOW OBSERVED WITH BATSE FROM GRB980923

T. W. Giblin[1,2], J. van Paradijs[1,3], C. Kouveliotou[2,4], V. Connaughton[5],
R.A.M.J. Wijers[6], M. S. Briggs[1,2], R. D. Preece[1,2], G. J. Fishman[2]

## ABSTRACT

In this *Letter*, we present the first evidence in the BATSE data for a prompt high-energy (25-300 keV) afterglow component from a $\gamma$-ray burst (GRB), GRB980923. The event consists of rapid variabilty lasting $\sim 40$ s followed by a smooth power law emission tail lasting $\sim 400$ s. An abrupt change in spectral shape is found when the tail becomes noticeable. Our analysis reveals that the spectral evolution in the tail of the burst mimics that of a cooling synchrotron spectrum, similar to the spectral evolution of the low-energy afterglows for GRBs. This evidence for a separate emission component is consistent with the internal-external shock scenario in the relativistic fireball picture. In particular, it illustrates that the external shocks can be generated during the $\gamma$-ray emission phase, as in the case of GRB990123.

*Accepted: 1999 August 12*

*Subject headings:* gamma rays: bursts

## 1. INTRODUCTION

The distinction between $\gamma$-ray bursts (GRBs) proper and their afterglows may be one between emission from shocks internal to the relativistic outflow and an external shock with a circumsource medium (Rees and Mészáros 1994; Sari and Piran 1997; Mészáros and Rees 1997). From an observational viewpoint, the relation between the burst proper and afterglow emissions is not well understood. However, the recent identification of a simultaneous optical counterpart to GRB990123 made with ROTSE (Akerloff et al. 1999) has shown that in some cases emissions from internal and external shocks can overlap, in agreement with the work of Sari and Piran (1999a).

One way to assess this relation has been the comparison of the 1-10 keV X-ray emission during the burst with that observed in the afterglow. Backward extrapolations of the *Beppo*SAX X-ray afterglow light curves to the decay part of the burst indicate that the late X-ray emission in the burst and the afterglow are consistent with a single power law decay curve indicating that the tail of the burst evolves continuously into the afterglow (Costa et al. 1997; Piro et al. 1998; Nicastro 1998; In't Zand 1998). These results appear to be in contradiction with the initial disappearance of X-ray emission in GRB780506, which was followed $\sim 400$ s later by their reappearance, supporting the case of afterglow emission disconnected from the burst (Connors and Heuter 1998). Elsewhere, evidence for extended hard $\gamma$-ray emission has been reported for $\sim 10\%$ of the bursts detected by PHEBUS (Tkachenko et al. 1995). OSSE has provided upper limits on high-energy ($> 300$ keV) post-burst emission from GRB950421 (Matz et al. 1996). Analysis of a subset of GRBs dubbed "FREDs" (Fast Rise Exponential Decay) from early in the BATSE mission has shown a softening trend in the decay of the burst (Bhat et al. 1994). More recently, Burenin et al. (1999) report GRANAT/SIGMA observations of a soft $\gamma$-ray tail lasting $\sim 1000$ s.

We present BATSE observations of GRB980923, which show that after a period of $\sim 40$ s of strong variability, the signal abruptly enters a phase of smooth decay. During this decay phase, which lasts $\sim 400$ s, the properties of the $\gamma$-ray emission are very similar to those of afterglows at lower energies. Our results support the idea that, in this case, the afterglow emission started during the burst, consistent with the theoretical prediction of early high-energy afterglow by Sari and Piran (1999b). The spectral evolution of this $\gamma$-ray afterglow indicates that it is the early, high-energy part of subsequent X-ray and optical afterglow.

## 2. GRB980923: BATSE OBSERVATIONS

On 1998 September 23 at 20:10:47.5 UT BATSE was triggered on the 64 ms time scale by a long and intense GRB (trigger 7113), shown in Figure 1. The burst was not in the field of view of the *Beppo*SAX WFC. RXTE/PCA made a single observation in stare mode in response to the BATSE Rapid Burst Response (Kippen et al. 1997) system, but observed no change in count rate. A full scan

[1]Department of Physics, University of Alabama in Huntsville, Huntsville, AL 35899, USA

[2]NASA Marshall Space Flight Center, SD50, Huntsville, AL 35812, USA

[3]Astronomical Institute "Anton Pannekoek", University of Amsterdam, & Center for High Energy Astrophysics, Kruislaan 403, 1098 SJ Amsterdam, The Netherlands

[4]Universities Space Research Association

[5]NRC, NASA Marshall Space Flight Center, SD50, Huntsville, AL 35812, USA

[6]Department of Physics and Astronomy, SUNY, Stony Brook, NY 11794-3800, USA

of the GRB error circle by RXTE/PCA was not possible at the time.

The event consists of complex variability lasting $\sim 40$ s, followed by a smooth emission tail. The 50-300 keV peak flux of the burst on the 64 ms time scale is $(1.16 \pm 0.02) \times 10^{-5}$ ergs sec$^{-1}$ cm$^{-2}$, ranking twelfth in brightness among all BATSE GRBs. The fluence of the burst ($> 25$ keV) is $(4.84 \pm 0.02) \times 10^{-4}$ ergs cm$^{-2}$, ranking third among all BATSE GRBs. The fluence in the tail ($> 40$ s) is $\sim 7\%$ of the total burst fluence.

## 3. TEMPORAL AND SPECTRAL ANALYSIS

Typically GRBs are short enough that prior and post background intervals can be chosen so that the behavior of the background during the burst emission interval can be estimated through interpolation. In the case of GRB980923, however, the duration of the emission tail is unknown, therefore routine background subtraction is not applicable. We use as background the average of the count rates registered when the spacecraft (CGRO) is positioned at the point closest in geomagnetic latitude to that at the time of the burst on days before and after the burst trigger, as described in Connaughton et al. (1999). Background rates were computed using both CONT (16 channel, 2.048 s time resolution) and DISCLA (4 channel, 1.024 s time resolution) data types for comparison.

The two detectors which have the highest burst count rates also have the smallest source angles to Vela X-1. The Vela pulsations were modeled using a 7 term harmonic Fourier expansion centered on a barycentric frequency equal to 3.546 mHz, as tabulated from BATSE pulsar monitoring (M. Finger, private communication). The model was fit to the background subtracted DISCLA data in channel 1 (25-50 keV) during a pre-burst interval ranging from $-405$ to $-5$ s and a post-burst interval from 300 to 1000 s, having a $\chi^2$/dof of 1.12 (1067 dof). Fourier spectra of the residual rates in the fitting intervals are consistent with that expected from Poisson fluctuations. We also modeled the pulsations in the CONT data (used for spectral modeling) using the same procedure and time intervals. Fits were made in each channel for channel 1 through 10 with an average reduced $\chi^2$ equal to 0.95.

### 3.1. *Temporal Modeling*

We modeled the tail count rates with a power law (PL) of the form $A(t - t_0)^\beta$. Separate fits were made in five energy ranges (25-50, 50-100, 100-300, 25-300, and $> 300$ keV) using the DISCLA count rate data from 40 to 298 s after the trigger time. For comparison, fits were also made using CONT data, binned in energy to match the DISCLA channel boundaries. A series of fits were made in each energy range for $t_0 = [-14.995, 32.109]$ at 1.024 s intervals using a $\chi^2$ minimization algorithm with two free parameters, $A$ and $\beta$, while the value of $t_0$ was held constant for each fit. From the fits in the energy ranges below 300 keV, we find best-fit (i.e., minimum $\chi^2$) values for $\beta$ in the range $-1.81$ to $-1.64$ (with typical uncertainties $\pm 0.03$) for $t_0$ in the range 9.6-12.1 s. For the high-energy ($> 300$ keV) emission we find $\beta = -1.85 \pm 0.53$ for $t_0 = 10.1$ s ($\chi^2$/dof = 0.2). The 99% confidence intervals in $t_0$ range from $-4$ to $+18$ s, and do not change much with energy. The best fit model in the 25-300 keV range using DISCLA data gives $\beta = -1.81 \pm 0.02$ ($\chi^2$/dof = 1.22) for $t_0 = 9.6$ s (see Figure 2). Both 68.3% (dashed) and 99% (solid) confidence intervals for $t_0$ are shown in Figure 2 with the 25-300 keV time history and the PL models from the range of $t_0$ values. The PL fits, and the obvious requirement that the PL emission cannot exceed the total burst signal, indicate that the PL decay started $\sim$ 20-25 s after the burst trigger. Note that there is no reason why $t_0$ for the afterglow should be 0, i.e. the time of trigger, since the (internal shock) GRB emission and (external shock) afterglow are physically different and thus somewhat independent in timing.

### 3.2. *Spectral Modeling*

For the spectral modeling we used the Vela-corrected CONT data (22-1880 keV) and constructed a single time-integrated spectrum for a time interval spanning 40.813 to 102.253 s in the tail. At the time of observation, the onboard LAD look-up table was in soft mode, mapping low energies into higher CONT channels and thus providing suitable statistics below 50 keV. To examine the spectral evolution in the tail we generated ten spectra with 8.192 s time resolution (four 2.048-second CONT bins) from 39.789 to 121.709 s in the tail. Although the tail of the burst appears to last beyond $\sim$250 s, we selected our source intervals such that the model fit parameters are reasonably constrained. The fits were made using the forward folding technique. The photon model that best represents the data was determined by comparing fits made with a single PL (2 free parameters) and a smoothly broken power law (SBPL) (4 free parameters) using the $\Delta\chi^2$ statistic (Band et al. 1997). We obtain $\Delta\chi^2 = 67$ with a chance probability of obtaining a value equal to or greater than $\Delta\chi^2$ of $\sim 10^{-15}$. Therefore, we used the SBPL to model the spectra for GRB980923.

The parameters of the SBPL are the low- and high-energy photon indices $\alpha_{\rm low}$ and $\alpha_{\rm high}$, and the break energy $E_{\rm b}$. From the time-integrated fit, we obtain $\alpha_{\rm low} = -1.66 \pm 0.04$, $\alpha_{\rm high} = -2.20 \pm 0.11$, and $E_{\rm b} = 203 \pm 59$ keV ($\chi^2$/dof = 1.06). The GRB function (Band et al. 1993) was also fit ($\chi^2$/dof = 1.07) giving nearly identical parameter values ($\alpha_{\rm GRB} = -1.59 \pm 0.05$, $\beta_{\rm GRB} = -2.192 \pm 0.14$, $E_{\rm p} = 271 \pm 52$), similar to values commonly found in GRB spectra (Preece et al. 1999). However, the GRB function proved to be less robust than the SBPL in the time resolved fits. From the ten fits made in the tail, we find that $\alpha_{\rm low}$ and $\alpha_{\rm high}$ do not vary significantly, with weighted average values $-1.68 \pm 0.03$ and $-2.09 \pm 0.07$, respectively. The break energy was held fixed in several of these fits to allow meaningful estimates of the photon indices. Therefore, we repeated the ten fits keeping $\alpha_{\rm low}$ and $\alpha_{\rm high}$ constant at their average values, allowing only the break energy and amplitude as free parameters. $E_{\rm b}$ decreases with time (see Figure 4), indicating that the spectrum retains a constant shape as it shifts in time to lower energies.

Time resolved spectra (2.048 s resolution) during the main burst emission were also modeled with a SBPL using CONT data corrected for deadtime effects and Vela pulsations. Figure 3 shows the evolution of $\alpha_{\rm low}$ and $\alpha_{\rm high}$ during the main burst and the tail. An abrupt change in the spectral form is quite evident where the

main burst emission drops sharply and the tail of the burst becomes detectable at $\sim 40$ s. The time integrated spectrum of the main burst gives GRB function parameters ($\alpha_{\rm GRB} = -0.61\pm0.01, \beta_{\rm GRB} = -2.95\pm0.08, E_{\rm p} = 364\pm3$), typical for GRBs (Preece et al. 1999).

Careful inspection of Figure 3 reveals a softening in the low-energy index, $\alpha_{\rm low}$, near 14 s, where the burst intensity drops to roughly the same level as observed in the tail (see Figure 1 and 2). Beyond $\sim 14$ s $\alpha_{\rm low}$ appears to maintain slightly steeper values, suggesting an overabundance of low-energy flux that was not present (or at least very weak) at the time of the burst trigger, which may be attributed to the rise of the afterglow since the decay must begin $\sim$ 20-25 s after the trigger time.

## 4. DISCUSSION

In the external shock scenario of the relativistic fireball model, electrons are accelerated to a PL energy distribution $N(\gamma_{\rm e})d\gamma_{\rm e} \propto {\gamma_{\rm e}}^{-p}d\gamma_{\rm e}$ by a forward shock generated when the relativistic shell encounters the surrounding medium, where $\gamma_{\rm e}$ is the electron Lorentz factor. The synchrotron spectrum of a relativistic shock with a PL electron distribution can be described by four PL regions segmented according to $\nu_{\rm a} < \nu_{\rm c} < \nu_{\rm m}$ in the *fast-cooling* regime, and $\nu_{\rm a} < \nu_{\rm m} < \nu_{\rm c}$ in the *slow-cooling* regime (Sari et al. 1998), where $\nu_{\rm a}$ is the self-absorption frequency, $\nu_{\rm c}$ is the cooling frequency, and $\nu_{\rm m}$ is the characteristic synchrotron frequency. For adiabatic evolution, $\nu_{\rm c}$ evolves as $t^{-1/2}$, while $\nu_{\rm m} \propto t^{-3/2}$ (Sari et al. 1996). In the fast-cooling regime, the evolution may be radiative, in which case $\nu_{\rm m} \propto t^{-12/7}$. Adopting the notation of Sari et al. (1998) and ignoring self-absorption, the observed spectral flux in the fast-cooling regime is given by

$$F_\nu = \begin{cases} F_{\nu,\max}(\nu/\nu_{\rm c})^{-1/2}, & \nu_{\rm c} < \nu < \nu_{\rm m}, \\ F_{\nu,\max}\left(\nu_{\rm m}/\nu_{\rm c}\right)^{-1/2}\left(\nu/\nu_{\rm m}\right)^{-p/2}, & \nu > \nu_{\rm m}. \end{cases} \quad (1)$$

Similarly, the flux in the slow-cooling regime can be written as

$$F_\nu = \begin{cases} F_{\nu,\max}(\nu/\nu_{\rm m})^{-(p-1)/2}, & \nu_{\rm m} < \nu < \nu_{\rm c}, \\ F_{\nu,\max}\left(\nu_{\rm c}/\nu_{\rm m}\right)^{-(p-1)/2}\left(\nu/\nu_{\rm c}\right)^{-p/2}, & \nu > \nu_{\rm c}. \end{cases} \quad (2)$$

Three characteristics of the synchrotron spectrum allow us to distinguish between the fast- and slow-cooling regimes: 1) the change in spectral slope across the break frequency, 2) the time dependence of the break frequency, and 3) the relation between the temporal and spectral PL indices.

For slow-cooling we expect a change in the spectral slope across $\nu_{\rm c}$ equal to $p/2 - (p-1)/2 = 0.5$; for fast-cooling, the change across $\nu_{\rm m}$ equals $p/2 - 1/2$. The value of $p$ can be obtained from $p/2 = -(\alpha_{\rm high} + 1)$, leading to $p = 2.4 \pm 0.11$, typical for afterglows. The expected change in slope in the fast-cooling regime then equals $0.7 \pm 0.11$. From the time-integrated spectral fit, we find a slope change of $0.54 \pm 0.12$; from the time-resolved fits we obtain an average change in slope of $0.42 \pm 0.09$. These values are in good agreement with slow-cooling, but do not exclude fast-cooling very strongly.

If we are observing a cooling break then we can expect the break energy to evolve as $t^{-1/2}$ (Sari et al. 1996) for adiabatic evolution. The time-dependent break energy was modeled with a PL of the form $E_0(t-t_0)^\delta$ in the same manner as the decay of the intensity. We find a PL index $\delta = -0.52 \pm 0.12$ ($\chi^2/{\rm dof} = 1.12$) for $t_0 = 32.109$ s (see Figure 4); slightly beyond the 99% confidence interval, but within a 99.9% interval and consistent with the PL decay starting $\gtrsim 20$ s after the trigger time. To obtain a fit with $\delta = -3/2$ or $\delta = -12/7$, corresponding to the two possible behaviors of $\nu_{\rm m} > \nu_{\rm c}$ (namely the adiabatic and radiative cases, respectively), would require $t_0$ to be negative, and is thus excluded by the data. We conclude that the break energy corresponds to the cooling frequency, i.e. the tail is in the slow-cooling regime.

If we insert the time dependence of $\nu_{\rm c}$ and $\nu_{\rm m}$ into the expressions for $F_\nu$ and let $\alpha \equiv (p-1)/2$ and $\alpha' \equiv p/2$, where $\alpha$ and $\alpha'$ are the low- and high-energy PL indices of the energy spectrum, then we have $F_\nu \propto \nu^{-\alpha}t^{-\frac{3}{2}\alpha}$ for $\nu < \nu_{\rm c}$ and $F_\nu \propto \nu^{-\alpha'}t^{-\frac{3}{2}\alpha'+\frac{1}{2}}$ for $\nu > \nu_{\rm c}$. Therefore, the relationships between the temporal and spectral indices are $\beta = -3\alpha/2$ for $\nu < \nu_{\rm c}$ and $\beta = -3\alpha'/2 + 1/2 = -3\alpha/2 - 1/4$ for $\nu > \nu_{\rm c}$. The values of $\alpha_{\rm low}$ and $\alpha_{\rm high}$ from the time integrated spectral fits give an expected values of $\beta = -0.99\pm0.04$ for the low frequency light curve ($\nu < \nu_{\rm c}$), and $\beta = -1.3\pm0.11$ for the high frequency light curve ($\nu > \nu_{\rm c}$). Similar values are derived when the average spectral indices are used. Since the PL decay must begin later than 20 s after the burst trigger, we can expect the decay index to be shallower than $-1.64$. For $t_0 = 32.109$ s we obtain $\beta = -0.98\pm0.02$ (25-50 keV), in agreement with the value computed from the spectral index and in accordance with the value of $t_0$ that gives the correct break energy PL index. Although this fit does not have the lowest $\chi^2$ ($\chi^2/{\rm dof} = 1.54$), it does satisfy the requirement that the PL can not exceed the total burst count rate. The same scenario holds for the high frequency light curve. Our measured value $\beta = -1.85 \pm 0.53$ in the high frequency regime ($> 300$ keV) is consistent with $\beta = -1.3$ derived from the spectral index.

In the fast-cooling regime, two cases must be considered. For adiabatic blast wave evolution, we expect $F_\nu \propto t^{(2-3p)/4} = t^{-1.3}$ above $\nu_{\rm m}$ which agrees with the measured high-energy decay. However, the expected behavior below $\nu_{\rm m}$ is $F_\nu \propto t^{-1/4}$, which strongly disagrees with the measured 25-50 keV PL index by at least 0.76 for all values of $t_0$. For radiative blast waves, the behavior above $\nu_{\rm m}$ is $F \propto t^{(2-6p)/7} = t^{-1.8}$, in agreement with the data; however, below $\nu_{\rm m}$ we expect $F \propto t^{-4/7}$, which also strongly disagrees with the data for all values of $t_0$. In summary, we conclude that fast-cooling scenarios with $\nu_{\rm c} < \nu_{\rm m}$ do not agree with the evolution of the tail of this burst.

## 5. CONCLUSION

We find similarities between the properties of GRB980923 and those of GRB920723 (Burenin et al. 1999). Both exhibit long soft $\gamma$-ray tails, however the tail of GRB920723 last longer by a factor 2 and decays less steeply ($\beta = -0.7$). Burenin et al. report a change

in spectral index equal to $\sim 0.8$, which is strikingly similar to the abrupt change we observe in $\alpha_{\rm low}$. From our spectral analysis we have been able to identify which blast wave evolution regime is favored in the production of the high-energy tail.

These results suggest a behavior not unlike that of afterglows observed at lower energies. In particular, the evolution of the spectrum in the tail of the burst appears to mimic the evolution of a synchrotron cooling break in the slow-cooling regime. This implies that the transition from fast to slow-cooling (i.e., when $\nu_{\rm m} = \nu_{\rm c}$) can take place on (short) time scales comparable to the duration of the burst. If the synchrotron emission from external shocks is the source of the "classical" afterglow, then our analysis provides evidence that, at least in some bursts, the afterglow may begin during the $\gamma$-ray emission phase and may reveal itself in the GRB light curves.

We thank Titus Galama and John Horack for comments on this manuscript. J.v.P. acknowledges support from NASA grant NAG 5-3247.

REFERENCES

Akerlof, C., W., and McKay, T., A., 1999, IAUC 7100
Band, D., et al., 1993, ApJ, 413, 281
Band, D., et al., 1997, ApJ, 485, 747
Bhat, P., N., et al., 1994, ApJ, 426, 604
Buerenin, R., A., et al., 1999, astro-ph/9902006
Connaughton, V., 1999, in preparation
Connors, A., and Hueter, G. J., 1998, ApJ, 501, 307
Costa, E., et al., 1997, Nature, 387, 783
Frontera, F., et al., 1998, ApJL, 493, L67
In't Zand, J. J. M., et al., 1998, ApJL, 505, L119
Kippen, R., M., et al., 1997, BAAS, 29, 2, 849
Matz, S., et al., 1996, AIP Conference Proceedings 384, pp. 52
Mészáros, P., and Rees, M. J., 1997, ApJ, 476, 232
Nicastro, L., et al., 1998, AAP, preprint
Piro, L., et al., 1998, AAP, 331, L41
Preece, R., et al., 1999, ApJS, in press.
Rees, M., and Mészáros, P., 1994, ApJ, 430, L93
Sari, R., Narayan, R., and Piran, T., 1996, ApJ, 473, 204
Sari, R., and Piran, T., 1997, ApJ, 485, 270
Sari, R., Piran, T., and Narayan, R., 1998, ApJL, 497, L17
Sari, R., and Piran, T., 1999a, ApJ, 517, L109
Sari, R., and Piran, T., 1999b, ApJ, 520, 641
Tkachenko, A., et al., 1995, Ap & SS, 231, 131

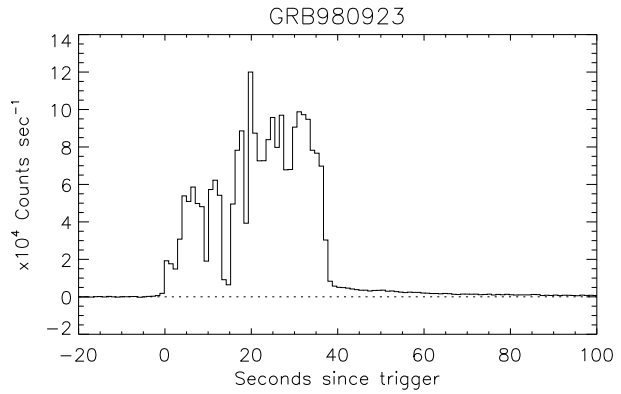


Fig. 1.— DISCLA time history of GRB980923 ($>$ 25 keV).

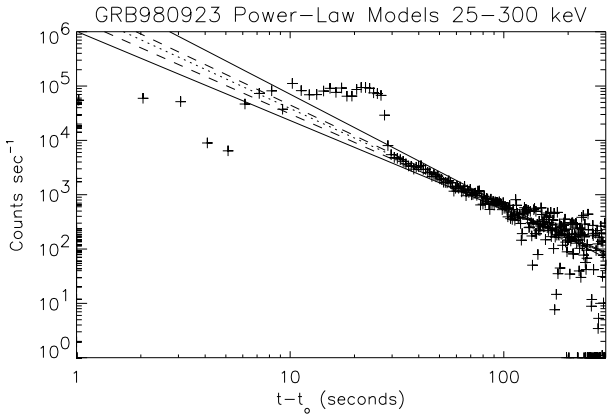


Fig. 2.— DISCLA time history of GRB980923 (25-300 keV) plotted logarithmically with a range of PL models extrapolated backwards in time through the burst proper. The confidence intervals for $t_0$ are designated by the dashed (68%) and solid (99%) curves. The dotted line is the fit for $t_0 = 9.581$ s ($\beta = -1.81 \pm 0.02$, $\chi^2/\mathrm{dof} = 1.22$).

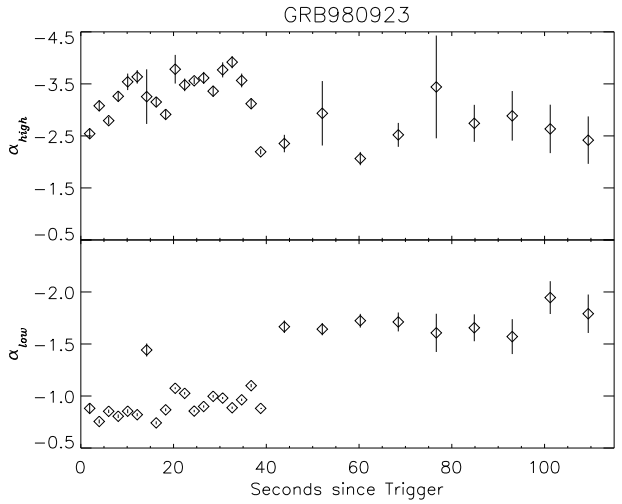


Fig. 3.— SBPL low- and high-energy photon indices (with one-sigma uncertainties) as a function of time since trigger.

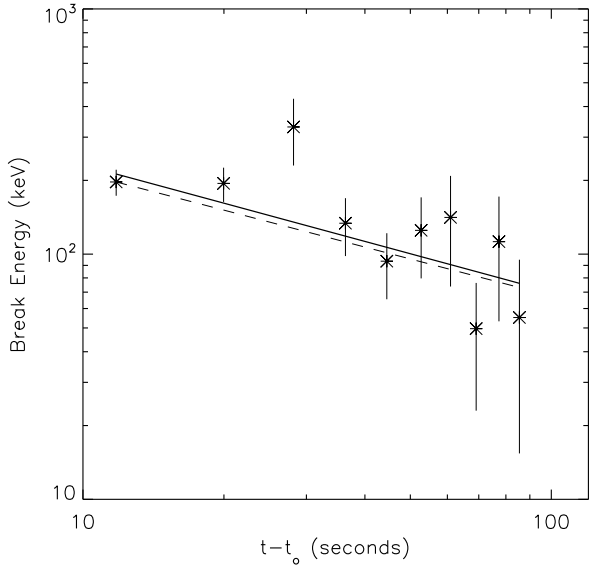


Fig. 4.— Break energy as a function of time since $t_0$ on logarithmic axes. The dashed line is the theoretical slope of $-1/2$ for synchrotron cooling. The solid line is the fitted PL slope $-0.52 \pm 0.12$ ($t_0 = 32.109$, $\chi^2/\mathrm{dof} = 1.12$).